CHEMISTRY
A EUROPEAN JOURNAL

DOI: 10.1002/chem.200800228

Superstructure-Dependent Optical and Electrical Properties of an Unusual Face-to-Face, π-Stacked, One-Dimensional Assembly of Dehydrobenzo[12]annulene in the Crystalline State

Ichiro Hisaki,*[a] Yuu Sakamoto,[a] Hajime Shigemitsu,[a] Norimitsu Tohnai,[a] Mikiji Miyata,*[a] Shu Seki,[b] Akinori Saeki,[c] and Seiichi Tagawa[c]

Abstract: To develop a novel π-conjugated molecule-based supramolecular assembly, we designed and synthesized trisdehydrotribenzo[12]annulene ([12]DBA) derivative **2** with three carboxyl groups at the periphery. Recrystallization of **2** from DMSO gave a crystal of the solvate **2**·3 DMSO. Crystallographic analysis revealed, to our surprise, that a face-to-face π-stacked one-dimensional (1D) assembly of **2** was achieved and that the DMSO molecule played a significant role as a "structure-dominant element" in the crystal. This is the first example of [12]DBA to stack completely orthogonal to the columnar axis. To reveal its superstructure-dependent optical and electrical properties, **2** and its parent molecule **1**, which crystallizes in a herringbone fashion, were subjected to fluorescence spectroscopic analysis and charge-carrier mobility measurements in crystalline states. The 1D stacked structure of **2** provides a red-shifted, broadened, weakened fluorescence profile ($\lambda_{max}=545$ nm, $\phi_F=0.01$), compared to **1** ($\lambda_{max}=491$ nm, $\phi_F=0.12$), due to strong interactions between the p orbitals of the stacked molecules. The charge-carrier mobility of the single crystal of **2**·3 DMSO, as well as **1**, was determined by flash photolysis time-resolved microwave conductivity (FP-TRMC) measurements. The single crystal of **2**·3 DMSO revealed significantly-anisotropic charge mobility ($\Sigma\mu=1.5\times10^{-1}\,cm^2V^{-1}s^{-1}$) along the columnar axis (crystallographic *c* axis). This value is 12 times larger than that along the orthogonal axis (the *a* axis).

Keywords: charge-carrier mobility · dehydroannulenes · fluorescence · pi interactions · solid-state structures

Introduction

Dehydrobenzo[*n*]annulenes ([*n*]DBAs), in which *n* denotes the number of π electrons in the cyclic pathway, are a family of carbon-rich π-conjugated cyclic systems involving benzene rings and acetylene units.[1] The chemistry of [*n*]DBAs was intensively investigated during the 1960s and 1970s mainly from the viewpoint of ring currents induced in cyclic π systems by magnetic fields. Subsequently, they have been studied from the various aspects, as unique organometallic ligands by Youngs et al.,[2] as precursors of carbon nanoparticles by Vollhardt and Bunz et al.,[3] and as partial units of non-natural carbon allotropes, such as the so-called graphyne and graphdiyne by Tobe and Haley et al.[4] Furthermore, various functionalized [*n*]DBAs have been synthesized, and their optical and optoelectronic properties have been investigated in solution for applications as functional materials.[5] To develop a significant property of [*n*]DBA in the solid state, on the other hand, the molecular arrangement is a crucial factor in addition to the molecular structure. So far,

[a] Dr. I. Hisaki, Y. Sakamoto, H. Shigemitsu, Dr. N. Tohnai, Prof. Dr. M. Miyata
Department of Material and Life Science
Graduate School of Engineering, Osaka University
2-1 Yamadaoka, Suita, Osaka, 565-0871 (Japan)
Fax: (+81) 6-6879-7404
E-mail: hisaki@mls.eng.osaka-u.ac.jp
miyata@mls.eng.osaka-u.ac.jp

[b] Prof. Dr. S. Seki
Division of Applied Chemistry
Graduate School of Engineering, Osaka University
2-1 Yamadaoka, Suita, Osaka, 565-0871 (Japan)

[c] Dr. A. Saeki, Prof. Dr. S. Tagawa
The Institute of Scientific and Industrial Research
Osaka University, 8-1 Mihogaoka, Ibaraki
Osaka, 567-0047 (Japan)

Supporting information for this article is available on the WWW under http://www.chemeurj.org/ or from the author.

some well-designed supramolecular architectures based on [*n*]DBA have been reported in crystals,[6] in liquid crystals,[7] in gels,[5f,g] in vesicles,[8] and on surfaces.[9] However, revealing the relationship between the superstructures and physical properties, such as optical, electrical, and electronic properties, and the development of novel functional materials based on [*n*]DBAs still remain as challenges.

Among the various molecular arrangements observed in supramolecular assemblies, a π-stacked, one-dimensional (1D) assembly is one of the most fundamental and fascinating ones, because the interactions between the p orbitals of the stacked molecules provide the pathway for charge or exciton migration to exhibit functional properties. Thus far, the optical, electrical, and electronic properties of π-stacked aggregates have been examined experimentally and theoretically for a large number of π-conjugated compounds including heterocyclic compounds, such as porphyrin and phthalocyanine, and polycyclic aromatic hydrocarbons (PAHs), such as triphenylene and hexabenzocoronene.[10] In most cases, π-stacked 1D aggregates are achieved in liquid crystals or in gels by using molecules with discotic cores the periphery of which is functionalized by long aliphatic chains. Moreover, to effectively achieve these, well-designed hydrogen bonds are also applied in some cases. For example, Müllen et al. reported the control of the molecular arrangement of hexabenzocoronene derivatives through the hydrogen bond of the urea moiety.[11]

In the crystalline state, on the other hand, a π-stacked 1D assembly is often difficult to achieve, because π–π interactions and CH–π interactions, which are unfavorable for π-stacked 1D assembly, play a significant role when discotic compounds such as PAHs crystallize. In connection with this, Desiraju and Gavezzotti have classified the molecular arrangements of PAHs into the following four categories, herringbone, sandwich herringbone, β, and γ structures, and they have established the relationship between molecular structure and molecular arrangement on the basis of the crystal structures of 32 PAHs.[12] They have proposed significant guidelines for the molecular arrangement of PAHs in crystals to rationalize and predict crystal structures of PAH from the molecular structures. However, the construction of face-to-face stacked 1D assembly in crystals has remained difficult, and even though large discotic compounds tend to stack in 1D columns, the cores are still tilted (in many cases, by 40–60°) with respect to the columnar axis.[13] In addition, organic crystals, especially single crystals, have other difficulties associated with material functionalization; for example, contingent and time-consuming growth processes and brittleness of the resulting crystals. However, crystallographically determined and thoroughly ordered molecular arrangements in organic crystals are fascinating from the viewpoint of not only fundamental chemistry, but also for the development of functional materials. Indeed, field-effect transistor (FET) properties of promising compounds, such as anthracene,[14] rubrene,[15] pentacene,[16] and others,[17] have been examined with the single crystals to develop organic semiconductor materials.

Trisdehydrotribenzo[12]annulene ([12]DBA) **1**,[18] which is the target molecule in this study, is also known to crystallize in a herringbone fashion; this arrangement is functionally

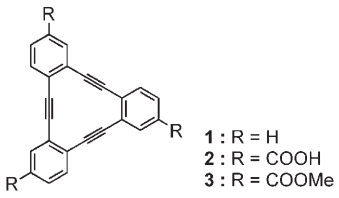

less useful arrangement due to small π–π interactions.[19] Thus, in order to improve optical and electrical properties of crystalline materials based on **1**, it is necessary to control its molecular arrangement in the solid state. To modulate the molecular arrangement of **1**, we introduced carboxyl groups into its periphery for the following two reasons. First, hydrogen bonds of the carboxyl groups, based on the supramolecular synthon theory,[20] can provide well-defined networked lattices to keep them in a co-planar arrangement. Second, any compound capable of hydrogen bonding with carboxylic groups can be examined by high-throughput screening to modulate the arrangement of the [12]DBA core. Indeed, we have successfully controlled the arrangement of anthracene chromophores in the crystalline state and have been able to change their emission properties on the basis of this crystal-engineering strategy.[21] In the present system, we serendipitously succeeded in constructing and crystallographically analyzing the face-to-face π-stacked 1D assembly of [12]DBA **2** in the crystalline state, in which the plane of **2** was completely orthogonal to the columnar axis. Although, Vollhardt et al. reported the face-to-face stacking of [12]DBA derivatives to form dimers,[22] the present system is the first example of [12]DBA derivatives to form a face-to-face stacked 1D columnar assembly. Furthermore, we revealed that the 1D assembly of **2** shows superstructure-dependent emission behavior, which yields a red-shifted, broadened, weakened fluorescence spectral profile, and significantly anisotropic charge mobility along the columnar axis ($\approx$12 times larger than that along the orthogonal axis).

Herein, we describe the synthesis of **2**, its crystal structure with the 1D columnar assembly, the role of the DMSO molecule as a "structure-dominant element", and its superstructure-dependent fluorescence and electrical properties. The fluorescence properties of **2** were evaluated both in solution and as a crystalline powder, and compared with those of its parent compound **1**. The charge-carrier mobility of the single crystal of **2**, as well as **1**, was estimated by flash photolysis time-resolved microwave conductivity (FP-TRMC) measurements.

Results and Discussion

Synthesis and crystallization of the [12]DBAs: [12]DBA **2** was synthesized with a 71% yield by the hydrolysis of the corresponding methyl ester **3**, which is derived from the iod-

ization of the diethyltriazene derivative **4**[23] with a 69% yield and desilylation followed by modified Castro–Stephens cyclization[24] of the resultant iodoethynylbenzene derivative **6** with a 39% yield in two steps, as shown in Scheme 1.

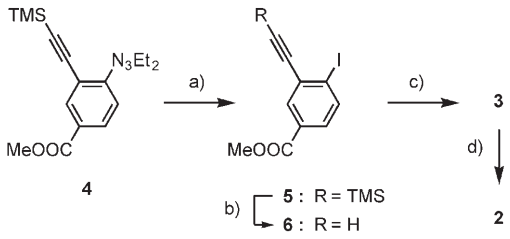

Scheme 1. Synthesis of [12]DBA **2**. a) CH_3I, 120°C, 17 h, 69%; b) TBAF, THF, RT; c) K_2CO_3, CuI, PPh_3, DMF, 120°C, 24 h, 39% for 2 steps; d) KOH, THF, RT, 19 h, 71%.

[12]DBA **1** was also prepared from 1-iodo-2-ethylylbenzene as the reference compound. To investigate the molecular arrangement in the solid state, [12]DBAs **1**, **2**, and **3** were then recrystallized from various organic solvents with or without a second component capable of hydrogen bonding. Slow evaporation of a solution of **1** in hexane/diisopropyl ether yielded pale yellow single crystals[25] in which molecule **1** was arranged in the same way as described in the literature; that is, in a herringbone fashion. In the case of **2**, recrystallization from DMSO yielded a yellow columnar single crystal **2**·3DMSO suitable for X-ray single-crystal analysis. To our surprise, molecules of **2** solvated with DMSO stack co-facially to give 1D columnar assembly. [12]DBA **3** yielded a needle-like crystal from dichloromethane. Its diameter was less than 0.01 mm, which is too thin for crystallographic analysis in our laboratory. However, powder X-ray diffraction (PXRD) patterns of the bulk crystal of **3** (see, Figure S1 in Supporting Information) exhibited a similar profile as that for **2**·3DMSO, indicating that molecules of **3** also aggregate in a π-stacked 1D columnar structure, though we have not described the aggregate of **3** in this manuscript.

Crystal structure of 1 and 2·3DMSO: In the crystalline state, **1** is packed in a herringbone fashion as already described in the literature (Figure 1a).[19] For a clear interpretation of the intermolecular interaction working in the crystal, the molecule of **1** in the crystal was drawn by the Hirshfeld surface[26] mapped with d_e between 1.0 and 2.6 Å, for which d_e denotes the distance from the surface to the nearest nucleus in another molecule. The surfaces (Figure 1b) show two sets of two significant orange spots (labeled i) on the benzene ring and the center of the trigonal structure of one side (left) and on the two benzene rings of the other side (right), as well as green flat regions (labeled ii) on the

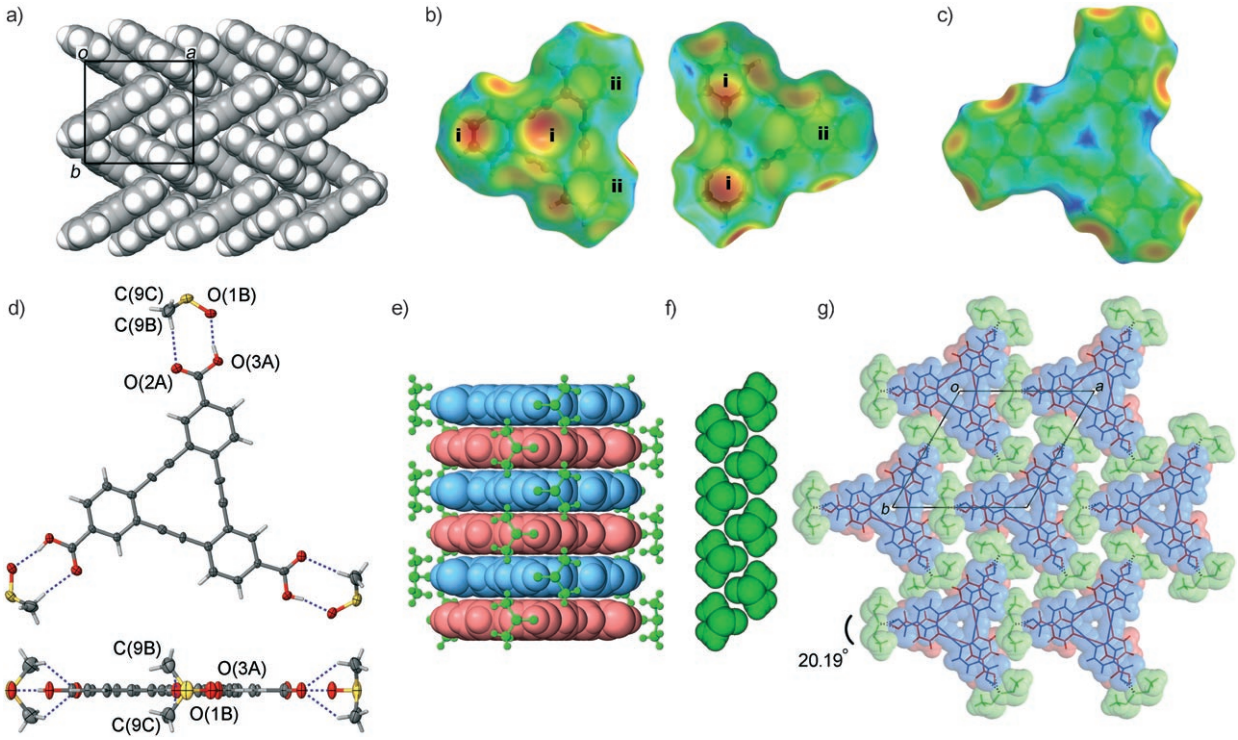

Figure 1. Structural features of **1** and **2** in the crystals. a) Packing diagram of **1** with a space-filling model. The Hirshfeld surface plots of b) **1** and c) **2**. The surfaces are mapped with d_e between 1.0 (red) and 2.6 (blue) Å. The orange spots labelled i and flat green regions labelled ii in b) and c) represent CH–π and π–π contacts, respectively. d) Diagrams of **2**·3DMSO with 50% thermal ellipsoids for non-hydrogen atoms. Symmetry codes: A: x, y, z; B: $1-y$, $1+x-y$, z; C: $1-y$, $1+x-y$, $1.5-z$. e) A side view of the 1D columnar assembly of **2**·3DMSO with a space-filling model for **2** and a ball-and-stick model for DMSO. f) A selected scaffold of the DMSO molecules. g) A hexagonal packing diagram of **2**·3DMSO. DMSO is depicted in green, **2** is depicted in red or blue in e)–g).

surface of both sides. The orange spots and the green regions indicate CH–π contacts and π–π stacking, respectively. Thus, these profiles imply that **1** is packed in the crystal with a large CH–π and tiny π–π interactions.

The crystal structure of **2**·3DMSO is shown in Figure 1d–g. The carboxylic group of **2** is solvated with the DMSO molecule through a strong hydrogen bond O(3A)H···O(1B), in which the distances between the O(1B) and O(3A) atoms and between the H and O(1B) atoms are 2.58 and 1.77 Å, respectively, and two weak hydrogen bonds C(9B)H···O(2A) and C(9C)H···O(2A), in which distances between H and O(2A) atoms and O(2A) and C(9B) or C(9C) atoms are 2.64 and 3.42 Å, respectively, and an angle of C(9B) or C(9C)−H···O(2A) is 137.4° (symmetry codes: A: x, y, z; B: $1-y$, $1+x-y$, z; C: $1-y$, $1+x-y$, $1.5-z$; Figure 1d). All atoms of the molecule **2**, including those of the carboxyl groups, and sulfur and oxygen atoms of DMSO are laid out on the same plane, leading to the C_{3h} symmetrical structure. The molecules stack in a face-to-face fashion, in which the plane of the [12]DBA cores is orthogonal to the columnar axis, to yield the A,B-type 1D columnar structure. The [12]DBA cores, A and B colored in red and blue in the figure, are staggered by 20.19°, and the distance between them is 3.52 Å (Figure 1e). The columns are parallel-packed into a hexagonal pattern (Figure 1g) through weak but favorable CH–S interactions. The Hirshfeld surface of **2**, mapped with d_e between 1.0 and 2.6 Å (Figure 1c), exhibits a large flat green region, indicating that the π–π interaction predominantly occurs over the whole π surface of the molecule. The orange spots on the edge of the molecule are due to CH–S contacts.

It is worth noting that the DMSO molecules bound to the periphery of **2** form well-fitted scaffolds with the intermolecular CH···O=S interactions (Figure 1f), preventing [12]DBA cores from forming CH–π interactions or slipped stacking. To confirm the steric effect of the DMSO molecules, other sulfoxides, such as ethylene-, methylethyl-, diethyl-, and dimethoxysulfoxides, were also subjected to co-crystallization with **2** under the same conditions as in the case of DMSO. No crystals were obtained from these systems: Ethylenesufoxide yielded a powder-like precipitate that did not exhibit any significant PXRD pattern, and the others also yielded amorphous films. This is probably due to steric misfit of the sulfoxides scaffolds. The approximate lengths of the sulfoxides are listed in Table 1. The d_{anti} value, which denotes the maximum diameter of the *trans*-conformation sulfoxides (Figure 2), of ethylenesulfoxide of 4.9 Å is much smaller than that for DMSO, which is 7.0 Å, while the others have larger values (8.2 to 9.4 Å). Thus, if **2** solvated by ethylenesulfoxide formed the 1D columnar assembly, the resulting structure should leave an unfavorable void space for crystallization. On the other hand, the three bulky sulfoxides probably do not allow for the construction of 1D stacked crystal structures like **2**·3DMSO, although the diameter of the *gauche* conformation (d_{gauche}) is comparable to that of DMSO. These indicate that DMSO molecules specifically work as the glue for construction of the face-to-face 1D structure of **2**. In addition, other molecules capable of participating in a hydrogen bond with **2** were subjected to co-crystallization with **2**. However, to our dismay, they have not yielded single crystals suitable for X-ray diffraction analysis yet.

Table 1. Approximate lengths[a] of sulfoxides subjected to co-crystallization with [12]DBA **2**.

Substituents	d_{anti} [Å]	d_{gauche} [Å]	Precipitates
R^1, R^2 = $-CH_2CH_2-$	4.9	–	powder
R^1 = R^2 = Me	7.0	–	single crystal
R^1 = Me, R^2 = Et	8.2	7.0	film
R^1 = R^2 = Et	9.4	7.9	film
R^1 = R^2 = OMe	8.6	–	film

[a] Molecular structures with *anti* conformation were optimized by HF/6–31G* level and those with *gauche* conformation were modeled based on MM calculations.

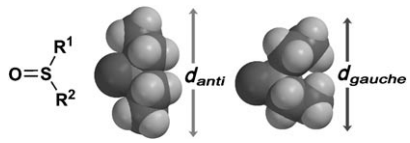

Figure 2. Space-filling models of diethylsulfoxides with *gauche* and *anti* conformations. The distances d_{gauche} and d_{anti} denote the diameters of the molecules in the respective conformations.

Stability of the crystal of 2·3DMSO: At ambient temperature, the DMSO molecules remained in the crystal when the crystals were placed under vacuum (≈1 Pa) for several hours. To evaluate the thermal stability of the crystal, thermal gravimetric (TG) analysis was carried out, given the fact that DMSO molecules are released from the crystal at about 111 °C (Figure S2 in the Supporting Information). Furthermore, the crystalline powder was subjected to DMSO desorption/absorption experiments, revealing that the crystal structure collapsed with loss of the DMSO molecules, while exposure of the resultant powder to DMSO vapors allowed for the recovery of the original structure. Figure 3 shows the change in the PXRD pattern of the crystalline powder upon desorption/absorption. The PXRD pattern of the crystalline powder of **2**·3DMSO (Figure 3b), which is in good agreement with that simulated from the single-crystal data (Figure 3a), changed into a broadened, different pattern upon removal of the DMSO molecules by heating at 130 °C for 1 h in vacuo (Figure 3c). The PXRD pattern in Figure 3c has a significantly broadened peak around $2\theta = 26.1°$ (3.41 Å) that can probably be attributed to the partly-surviving π stacked aggregate of **2**. On the other hand, the corresponding peak in the pattern in Figure 3b is observed at $2\theta = 25.0°$ (002 diffraction peak), the d-spacing of which is 3.56 Å, indicating that the 1D assembly of **1** shrinks by about 4% along the columnar axis (c axis in the crystal structure) by replacement of the appended DMSO molecules, which is also implied by its solid-state fluorescent spectrum (vide infra).

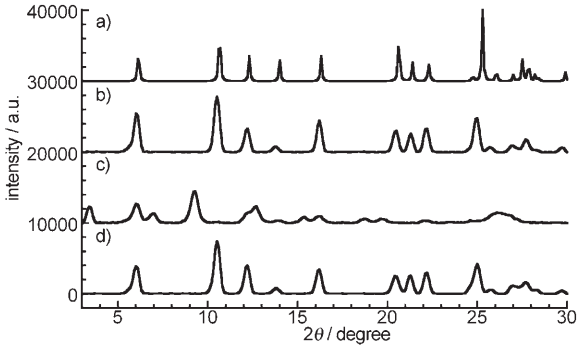

Figure 3. Change in the PXRD patterns of **2**·3 DMSO upon desorption/absorption. a) Simulated pattern from single-crystal X-ray diffraction data. b) Observed pattern of crystalline powder, c) after heating at 130 °C for 1 h in vacuo, and d) after exposure to vaporous DMSO at 40 °C for 43 h

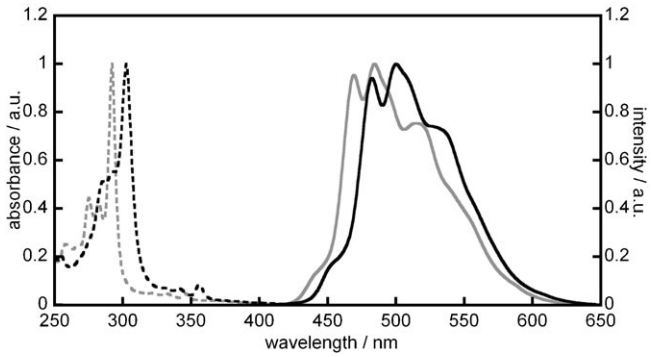

Figure 4. Normalized UV/Vis (dashed line) and fluorescence (solid line) spectra of **1** (gray) and **2** (black) in solution. The concentrations of **1** and **2** in the solutions are 5.0 and 2.9 μM, respectively. Excitation wavelengths for **1** and **2** are 303 and 292 nm, respectively.

Comparison of the low angle diffraction peaks between the patterns in Figure 3b and c indicates that rearrangement of the columnar structure also occurred upon removal of the DMSO molecules. Especially, the *d*-spacing (26 Å) of a new peak at $2\theta = 3.4°$ in the pattern in Figure 3c is consistent with the length of the dimeric species of **2** derived by the self-complementary hydrogen bond of carboxylic moieties. Interestingly, when the destructured powder was exposed to DMSO vapor at 40 °C for 43 h, the original PXRD pattern completely recovered as shown in the pattern in Figure 3d. Thus, these results clearly indicate that DMSO is an excellent "structure-dominant element" for construction of the crystal with 1D columnar assembly of **2**.

Optical properties of the DBAs: The 1D π-stacked structure is especially attractive for examining the optical and electrical properties, as reported for PAHs.[10] To reveal the superstructure-dependent optical properties of [12]DBA systems, the electronic spectra of **2** were measured in the crystalline state and in DMSO, and compared with those of the parent compound **1**. First, to clarify self-association behaviors of **1** and **2** in DMSO, ^{1}H NMR spectra of **1** and **2** were measured in various concentrations, yielding no changes in chemical shifts up to concentrations of 2 mM (see Figures S3 and S4 in the Supporting Information). Similarly, the UV/Vis spectra of **1** and **2** do not show any hypochromic spectral change of the absorption bands in the range of 5.9–1.5 μM and 10–2.5 μM, respectively (see Figures S5 and S6 in the Supporting Information). These results indicate that **1** and **2** are well dispersed in the DMSO. Next, we compare the optical properties of **1** and **2**. In solution, **1** and **2** show absorption maxima at 292 and 303 nm, respectively, and lower energy bands at around 345 and 356 nm, respectively (Figure 4). The spectral profile of **2** is similar to that of **1**, but is slightly red-shifted by about 10 nm. The fluorescence emission spectrum of **2** with bands at 483, 500, and approximately 530 nm also shows a spectral profile similar to that of **1** with 469, 484, and 515 nm, but is red-shifted by about 15 nm. The fluorescence quantum yields of **1** and **2** are 0.15 and 0.07, respectively, based on quinine sulfate reference. The cause of the observed red-shifted absorption spectrum of **2** was determined by the time-dependent density functional theory (TDDFT) calculation at the B3LYP/6-31+G* level as shown in Figure 5.[27] [12]DBA **2** shows the signals ascribed

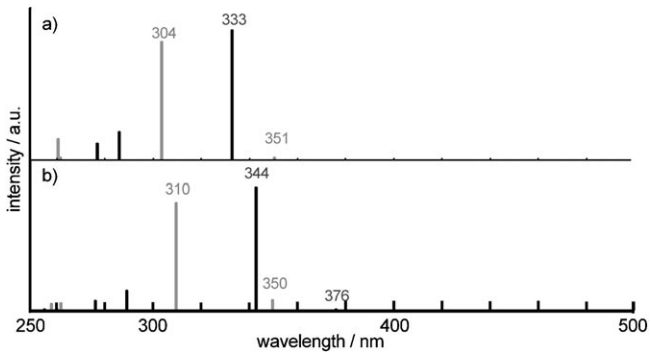

Figure 5. Calculated UV/Vis spectra of **1** (gray bar) and **2** (black bar) a) in vacuo and b) in DMSO. The excitation energy has been calculated with the TDDFT method using the B3LYP/6-31+G* basis set. The structures are optimized at the B3LYP/6–31G* level. The values in the DMSO solutions were obtained using the IEFPCM scheme.

to π–π* transitions (HOMO→LUMO+1 and HOMO−1→LUMO) at 333 nm which is red-shifted by 29 nm relative to the corresponding signal of **1** (304 nm). Moreover, calculation with the integral equation formalism version of the polarizable continuum model (IEFPCM)[28] accounting for the electrostatic interactions between the [12]DBA molecules and the solvent; that is, DMSO, further gives a red-shifted value of 34 nm in the absorption spectrum of **2**. Thus, although quantitative evaluation is difficult due to the large difference between the observed and calculated absorption spectra, the calculation results qualitatively indicate that the observed red-shifted absorption spectrum of **2** is due to both the effect of perturbation of the carboxyl groups and the solvent effect of DMSO.

In the crystalline state, although the relative difference in the wavelength between the maximum absorption bands of

1 and **2** remains at about 10 nm, the spectral profiles of **1** and **2** are strongly broadened and red-shifted by approximately 120 nm relative to those found in solution, as shown in Figure 6, resulting in much smaller values of the Stokes

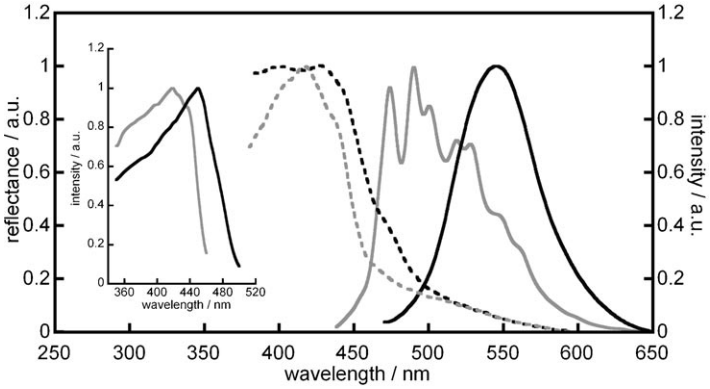

Figure 6. Normalized UV/Vis (dashed line), fluorescence (solid line), and excitation (inset) spectra of **1** (gray) and **2**·3 DMSO (black) in the crystals. Excitation wavelengths for the fluorescence spectra of **1** and **2** are 449 and 414 nm, respectively. Excitation spectra of **1** and **2** are recorded at 491 and 500 nm, respectively.

shift than those in the solution due to rigidly packed crystal structures. The fluorescence excitation spectra of **1** and **2** in Figure 6 (inset) are in agreement with their absorption spectra. It is worth noting that the fluorescence spectra of **1** and **2** show completely different profiles. The spectrum of the crystalline solid of **1** shows a more unambiguous vibrational structure (bands at 474, 491, 500, 519 and 528 nm) than that in solution, though they lie in a similar wavelength region. This is caused by molecular packing with tiny π–π interactions and/or emission from two or more excitation states. On the other hand, the crystalline solid of **2**·3 DMSO shows a strongly broadened, structureless spectrum ($\lambda_{max}=545$ nm) that is red-shifted by nearly 50 nm relative to the maximal emission band in the solution. This indicates that the molecule has π–π interaction with the adjacent molecule and that the exciton may delocalize along the π–π stacked 1D columns to form excited oligomeric species. Indeed, the emission quantum efficiency of the crystalline **2**·3 DMSO ($\phi_F=0.01$) is much smaller than that of **1** ($\phi_F=0.12$). Furthermore, the powder sample after removal of the DMSO molecules (Figure 3c), which implies shorter π-stack distance than **2**·3 DMSO, exhibits an emission maximum at 550 nm (Figure S7 in the Supporting Information) which is slightly red-shifted compared to **2**·3 DMSO due to stronger interactions between the neighboring molecules. These results strongly indicate that the arrangement of [12]DBA cores crucially affects the solid-state optical properties.

Electrical properties of the DBAs: The molecular arrangement of π-conjugated discotic compounds is significant for the conductive properties of the crystal. Especially, one-dimensional conductivity of materials depends on the interaction between the delocalized π orbitals of adjacent [12]DBAs. To evaluate charge mobility of the crystals **1** and **2**·3 DMSO, their single crystals were subjected to flash photolysis time-resolved microwave conductivity (FP-TRMC) measurements.[29] The TRMC technique, which can predict the nanometer-scale mobility of charge carriers generated by laser pulse irradiation under a low oscillating microwave electric field, has been recently applied to assess the instinct mobility of π-conjugated polymers and π–π-stacked discotic materials, because the technique is not affected by chemical or physical defects in the material or the organic/metal-electrode interface.[30] Moreover, we investigated the anisotropy of the charge transport in the single crystals, because although the present system has a sophisticated π-stacked 1D column, the column is insulated from the neighbors only by DMSO molecules. In general, in the case of liquid crystal[31] and graphitic nanotube[30d] systems of discotic cores having long alkyl chains, peripheral long hydrocarbon chains insulate the conductive parts, resulting in highly anisotropic 1D charge transport, while in the case of crystals reported so far, the anisotropy tends to remain relatively low (the ratio is within five) due to close packed π-conjugated molecules.

Figure 7 displays photographs of the single crystals, their crystalline indices, and the corresponding molecular arrangements. The crystal of **1** exhibits a block-like shape with dimensions of $0.4\times0.7\times1.0$ mm and the crystal of **2**·3 DMSO exhibits a hexagonal column-like shape with dimensions of

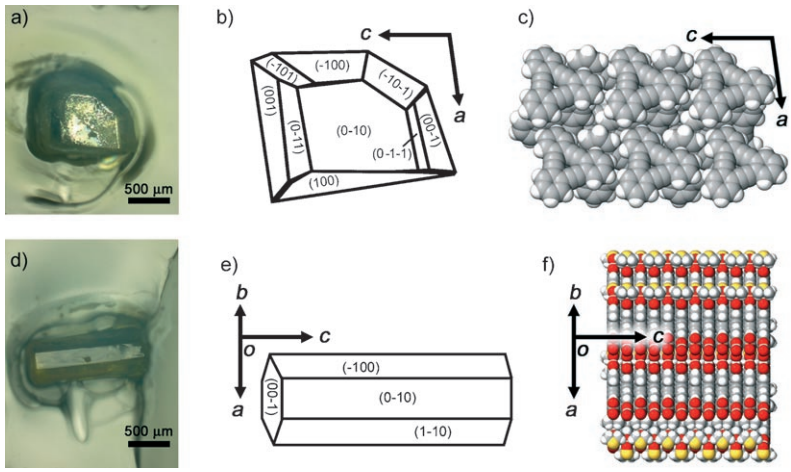

Figure 7. Single crystals of **1** and **2**·3 DMSO used in the PF-TRMC measurement. Photograph of the crystals a) **1** and d) **2**·3 DMSO. Crystal shapes with indices for b) **1** and e) **2**·3 DMSO. Molecular arrangements of c) **1** and f) **2**·3 DMSO corresponding to the photographs.

$0.3 \times 0.3 \times 1.3$ mm. The microwave electric field was applied along the crystallographic *a* and *c* axes directions in the single crystals of both **1** and **2**·3DMSO to investigate anisotropic conductivity. With regards to the p-orbital overlapping of the annulene molecules, compound **1**, which aligns co-planarly along the *c* axis, is slightly π-stacked along the *a* axis, while **2**, which is packed co-planarly in the *ab* plane, π stacks to form a 1D structure along the *c* axis, as described above.

Figure 8 shows the kinetic traces of the conductivity ($\phi\Sigma\mu$) of the single crystals of **1** and **2**·3DMSO obtained from TRMC measurements, in which ϕ and $\Sigma\mu$ denote photocarrier generation yield (quantum efficiency) and sum of mobilities for negative and positive carriers, respectively. The transient curves of **2** are shown in Figure 8a; the gray and black curves correspond to the conductivity along the crystallographic *a* and *c* axes, respectively. Upon irradiation of a laser pulse with an excitation wavelength of 355 nm, the single crystal of 2·3DMSO revealed a strong transient conductivity $\phi\Sigma\mu$ with a peak of $6.9 \times 10^{-3}\,cm^2V^{-1}s^{-1}$ at 81 ns after irradiation along the *c* axis and weak conductivity with a peak of $6.0 \times 10^{-4}\,cm^2V^{-1}s^{-1}$ at 106 nm along the *a* axis. On the other hand, the single crystal of **1** showed only a weak transient conductivity peak of $1.9 \times 10^{-3}\,cm^2V^{-1}s^{-1}$ along the *a* axis and no conductivity along the *c* axis.

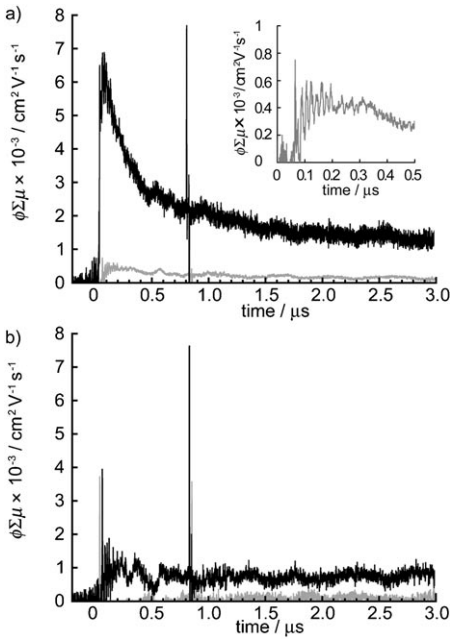

Figure 8. Conductivity transients for the single crystals of a) **2**·3DMSO and b) **1**. The transients colored by gray and black in a) are along the *a* and *c* axes, respectively. Those by gray and black in b) are along the *c* and *a* axes, respectively. The inset in a) shows the partially expanded curve of the conductivity of **2**·3DMSO along the *c* axis. The spike observed at 0.8 μs is just noise.

To determine the value of the charge-carrier mobility $\Sigma\mu$, the value of ϕ was determined by the conventional direct-current current integration (DC-CI) method using thin films (≈ 3 μm thick) of **1** and **2** that were cast from solutions of the samples in DMSO on Al substrates and overcoated by an Au semitransparent electrode, under excitation at 355 nm with a power density of $5\,mJ\,cm^{-2}$. It should be noted that the transient was obtained under an applied +5 V bias voltage between the electrode (Figure S8 in the Supporting Information), while no transient was observed under a negative bias, suggesting that the major charge carriers are holes. The value for **1** (6.5%) was slightly larger than that for **2** (4.5%), corresponding to the fact that the HOMO level of **1** (−5.30 eV) is higher than that of **2** (−5.82 V) or **2** solvated by DMSO (−5.47 eV) (Figure S9 in the Supporting Information). Assuming that the values of ϕ in the single crystals are the same as those in the films, the single crystal of **1** exhibits the minimum mobility of $3.3 \times 10^{-2}\,cm^2V^{-1}s^{-1}$ along the *a* axis and the single crystal of **2**·3DMSO exhibits minimum mobilities of 1.5×10^{-1} and $1.3 \times 10^{-2}\,cm^2V^{-1}s^{-1}$ along the *c* and *a* axes, respectively.[32]

It is not easy to compare the values obtained in this study with the reported values in other promising systems such as rubrene by the time of flight or field-effect transistor methods.[15,17] However, the single crystal of **2**·3DMSO yielded a larger value compared with that of the single crystal of rubrene ($\Sigma\mu = 5.2 \times 10^{-2}\,cm^2V^{-1}s^{-1}$) obtained by the FP-TRMC method.[30e,33] Furthermore, it is worth noting that significant anisotropy of charge transport is observed in the single crystal of **2**·3DMSO. The mobility along the *c* axis is ≈ 12 times larger that that along the *a* axis, although the [12]DBA molecules lie coplanarly in the crystallographic *ac* plane and are insulated from the adjacent molecules only by DMSO molecules. The observed high anisotropic conductivity is presumably due to not only spatial but also the energetic barrier of the DMSO for the charge-carrier transport. The anisotropic effect observed in the present system is significantly higher than that in reported crystalline systems[17a] and comparable to the graphitic systems.[30e,31] Thus, [12]DBA **2** is expected to be another candidate for organic semiconductors.

Conclusion

A face-to-face stacked 1D columnar assembly composed of [12]DBA macrocyclic cores was successfully constructed by co-crystallization of the carboxylic derivative **2** with DMSO, and was characterized by single-crystal X-ray analysis. The 1D stacked structure of **2** in the solid state was revealed to show the red-shifted, broadened, weakened fluorescence spectrum, relative to the parent compound **1**, which crystallizes in a herringbone fashion with only a very small amount of π orbital overlap. We also revealed that the single crystal of **2**·3DMSO has significantly anisotropic charge mobility ($\Sigma\mu = 1.5 \times 10^{-1}\,cm^2V^{-1}s^{-1}$) along the columnar axis. The value is 12 times larger than that along the orthogonal axis. Thus, [12]DBA **2** can be another candidate for organic semiconductor materials. These characteristics are strongly dependent on the supramolecular structure in the assemblies.

Experimental Section

General methods: ^{1}H and ^{13}C spectra were measured by a JEOL spectrometer (270 MHz for ^{1}H and 67.5 MHz for ^{13}C). MS data were obtained from a JEOL JMS-700 instrument. UV/Vis spectra in the solid state and in solution were measured on a JASCO V-550 spectrometer. Thermogravimetric analysis was performed on a Rigaku TAS100 system and Rigaku Thermoplus TG8120 with about 10 mg of sample from 30 to 250 °C at a heating rate of 5 °C min^{-1}. Emission spectra in the solid state and in solution were measured using a JASCO FP-6500 spectrofluorometer with an accessory and a cell for solid samples from JASCO. FT-IR spectra of the synthesized compounds in a KBr pellet were recorded using a Horiba FT-720 spectrometer.

Crystal structure determination: X-ray diffraction data were collected on a Rigaku R-AXIS RAPID diffractometer with a 2D area detector using graphite-monochromatized $Cu_{K\alpha}$ radiation ($\lambda = 1.54187$ Å). Direct methods (SIR-97) were used for the structure solution.[34] All calculations were performed with the observed reflections [$I > 2\sigma(I)$] by the program CrystalStructure crystallographic software packages[35] except for refinement, which was performed using SHELXL-97.[36] All non-hydrogen atoms were refined with anisotropic displacement parameters and hydrogen atoms were placed in idealized positions and refined as rigid atoms with the relative isotropic displacement parameters.

Crystal data ***1***: $C_{24}H_{12}$, $M_r = 300.36$, $0.8 \times 0.8 \times 0.6$ mm, $a = 11.7275(3)$, $b = 10.9297(3)$, $c = 12.4438(3)$ Å, $\alpha = 90°$, $\beta = 98.4239(18)°$, $\gamma = 90°$, $V = 1577.81(7)$ Å^3, $T = 213$ K, monoclinic, space group $P2_1/c$ (No. 14), $Z = 4$, $\mu(Cu_{K\alpha}) = 0.5492$ mm^{-1}, $\rho_{calcd} = 1.264$ g cm^{-3}, 8293 reflections collected, 2764 unique ($R_{int} = 0.087$) reflections, The final $R1$ and $wR2$ values were 0.052 [$I > 2.0\sigma(I)$] and 0.124 (all data), respectively.

Crystal data ***2**·3DMSO*: $C_{33}H_{30}O_9S_3$, $M_r = 666.77$, $0.2 \times 0.2 \times 0.6$ mm, $a = 16.5993(4)$, $b = 16.5993(4)$, $c = 7.0364(3)$ Å, $\alpha = 90°$, $\beta = 90°$, $\gamma = 120°$, $V = 1679.05(8)$ Å^3, $T = 213$ K, hexagonal, space group $P\bar{6}2c$ (No. 190), $Z = 2$, $\mu(Cu_{K\alpha}) = 2.458$ mm^{-1}, $\rho_{calcd} = 1.319$ g cm^{-3}, 16108 collected, 1124 unique ($R_{int} = 0.074$) reflections, The final $R1$ and $wR2$ values were 0.069 [$I > 2.0\sigma(I)$] and 0.173 (all data), respectively.

CCDC-679449 (**1**) and 664534 (**2**) contain the supplementary crystallographic data for this paper. These data can be obtained free of charge from The Cambridge Crystallographic Data Centre via www.ccdc.cam.ac.uk/data_request/cif.

Powder X-ray diffraction (PXRD): PXRD data were collected on a Rigaku RINT-1100 or RINT-2000 using graphite-monochromatized Cu Kα?radiation ($\lambda = 1.54187$ Å) at room temperature.

Flash-photolysis time-resolved microwave conductivity (FP-TRMC) measurements: Nanosecond laser pulses from a Nd:YAG laser (third harmonic generation, THG (355 nm) from Spectra Physics, GCR-130, FWHM 5–8 ns) were used as excitation sources. The power density of the laser was set at 1.0–20 mJ/cm^2. For time-resolved microwave conductivity (TRMC) measurements, the microwave frequency and power were set at ≈9.1 GHz and 3 mW, respectively, so that the motion of the charge carriers was not disturbed by the low electric field of the microwaves. The TRMC signal picked up by a diode (rise time < 1 ns) is monitored by a digital oscilloscope. All the above experiments were carried out at room temperature. The transient photoconductivity ($\Delta\sigma$) of the samples is related to the reflected microwave power ($\Delta P_r/P_r$) and sum of the mobilities of charge carriers as given in Equations (1) and (2).

$$\langle \Delta\sigma \rangle = \frac{1}{A} \frac{\Delta P_r}{P_r} \quad (1)$$

$$\Delta\sigma = e \sum \mu\phi N \quad (2)$$

In these equations A, e, ϕ, N, and $\Sigma\mu$ represent a sensitivity factor, elementary charge of an electron, photocarrier generation yield (quantum efficiency), number of absorbed photons per unit volume, and sum of mobilities for negative and positive carriers, respectively. The number of photons absorbed by the sample was estimated based on steady state absorption spectra of the thin solid films of the corresponding compounds. The values of ϕ for the films of **1** and **2** were determined by conventional DC current integration using 3 μm thick films sandwiched by Al and semi-itransparent-Au electrodes under excitation at 355 nm with a power density of 5.0 mJ cm^{-2}. Other details of the apparatus are described elsewhere.[30]

Methyl 4-iodo-3-trimethylsilylethynylbenzenoate (5): Diethyltriazene **4** (100 mg, 0.302 mmol), which was synthesized according to the report by Haley et al.,[23] was dissolved in methyl iodide (2 mL) in an autoclave under a nitrogen atmosphere. The reaction vessel was placed in an oil bath at 120 °C for 17 h. After cooling to room temperature, the solvent was removed under reduced pressure. The residue was subjected to column chromatography on silica gel (dichloromethane) and washed with $Na_2S_2O_3$ aqueous solution to yield **5** (74.6 mg, 69 %) as a yellow crystalline powder. M.p. 45 °C; ^{1}H NMR (270 MHz, $CDCl_3$): $\delta = 8.08$ (d, $J = 2.2$ Hz, 1H; ArH,), 7.92 (d, $J = 8.3$ Hz, 1H; ArH), 7.60 (dd, $J = 2.0$, 8.2 Hz, 1H; ArH), 3.91 (s, 3H; OCH_3), 0.29 ppm (s, 9H, $SiCH_3$); ^{13}C NMR (67.5 MHz, $CDCl_3$): $\delta = 165.8$, 138.9, 133.3, 130.1, 129.9, 129.8, 107.2, 105.5, 100.0, 52.4, −0.2 ppm; IR (KBr): $\tilde{\nu} = 2954$, 2160, 1720 cm^{-1}; HR-MS (FAB): *m/z* calcd for $[M]^+$ $C_{13}H_{15}O_2SiI$: 357.9886; found: 357.9880.

Dehydrobenzo[12]annulene 3: A 1 M solution of tetrabutylammonium fluoride in THF (0.7 mL, 0.7 mmol) was added to a solution of **5** (500 mg, 1.40 mmol) dissolved in THF (20 mL). After stirring for 1 h at room temperature, the solvent was removed under reduced pressure. The residue was extracted with dichloromethane and washed with water. After drying the organic layer with anhydrous $MgSO_4$, the solvent was evaporated under reduced pressure to yield iodophenylacetylene **6** as an oil. The resulting material was used for the following step without further purification. A solution of iodophenylacetylene dissolved in DMF (5 mL) was added to a mixture of K_2CO_3 (580 mg, 4.20 mmol), CuI (80 mg, 0.42 mmol), PPh_3 (110 mg, 0.419 mmol). The mixture was stirred for 24 h in an oil bath at 120 °C under a nitrogen atmosphere. The mixture was poured into H_2O and extracted with chloroform. After drying the organic layer over anhydrous $MgSO_4$, the solvent was evaporated under reduced pressure. The residue was purified by column chromatography on silica gel (chloroform) to yield **3** (86.1 mg, 39 %) in the form of an ocher powder. M.p. (decomp) 240 °C; ^{1}H NMR (270 MHz, $CDCl_3$): $\delta = 8.03$ (s, 3H; ArH), 7.88 (d, $J = 8.1$ Hz, 3H; ArH), 7.43 (d, $J = 8.1$ Hz, 3H; ArH), 3.94 ppm (s, 9H; OCH_3); ^{13}C NMR (67.5 MHz, $CDCl_3$): $\delta = 165.4$, 133.3, 132.1, 130.7, 130.2, 129.9, 126.3, 94.8, 92.7, 52.5 ppm; IR (KBr) $\tilde{\nu} = 3448$, 2923, 1720 cm^{-1}; HR-MS (EI): *m/z* calcd for $[M]^+$ $C_{30}H_{18}O_6$: 474.1103; found: 474.1099.

Dehydrobenzo[12]annulene 2: 10 % KOH aqueous solution (10 mL) was added **t**o a solution of DBA **3** (86.1 mg, 0.181 mmol) in THF (20 mL). The mixture was stirred for 19 h at room temperature. The aqueous layer was separated and a 2 M HCl aqueous solution was added to the aqueous layer. The resulting precipitation was gathered by a centrifuge, rinsed with water several times, and dried under vacuum to yield **2**, (55.5 mg, 71 %) as an orange powder. M.p. (decomp) 207 °C; ^{1}H NMR (270 MHz, [D_6]DMSO): $\delta = 13.33$ (br s, 3H; OH), 7.92 (d, $J = 1.4$ Hz, 3H; ArH), 7.85 (dd, $J_1 = 1.8$, 8.2 Hz, 3H; ArH), 7.61 ppm (d, $J = 8.4$ Hz, 3H; ArH); ^{13}C NMR (67.5 MHz, [D_6]DMSO): $\delta = 165.5$, 132.7, 132.5, 131.4, 130.2, 129.2, 125.2, 94.2, 92.3 ppm; IR (KBr) $\tilde{\nu} = 3401$, 2924, 2214, 1689 cm^{-1}; HR-MS (EI): *m/z* calcd for $[M]^+$ $C_{27}H_{12}O_6$: 432.0634; found: 432.0639.

Acknowledgement

This work was supported by a Grant-in-Aid for Scientific Research from the Ministry of Education, Culture, Sports, Science, and Technology, Japan.

[1] For recent reviews, see; a) C. S. Jones, M. J. O'Connor, M. M. Haley, in *Acetylene Chemistry* (Eds.: F. Diederich, P. J. Stang, R. R. Tykwinsky), Wiley-VCH, Weinheim, **2005**, pp. 303–385; b) U. H. F. Bunz, Y. Rubin, Y. Tobe, *Chem. Soc. Rev.* **1999**, *28*, 107–119; c) I. Hisaki,

M. Sonoda, Y. Tobe, *Eur. J. Org. Chem.* **2006**, 833–847; d) E. L. Spitler, C. A. Johnson II, M. M. Haley, *Chem. Rev.* **2006**, *106*, 5344–5386.

[2] a) J. D. Ferrara, C. Tessier-Youngs, W. J. Youngs, *J. Am. Chem. Soc.* **1985**, *107*, 6719–6721; b) J. D. Ferrara, A. Djebli, C. Tessier-Youngs, W. J. Youngs, *J. Am. Chem. Soc.* **1988**, *110*, 647–649; c) A. Djebli, J. D. Ferrara, C. Tessier-Youngs, W. J. Youngs, *J. Chem. Soc. Chem. Commun.* **1988**, 548–549; d) J. D. Ferrara, C. Tessier-Youngs, W. J. Youngs, *Inorg. Chem.* **1988**, *27*, 2201–2202.

[3] a) K. P. Baldwin, A. J. Matzger, D. A. Scheiman, C. A. Tessier, K. P. C. Vollhardt, W. J. Youngs, *Synlett* **1995**, 1215–1218; b) R. Boese, A. J. Matzger, K. P. C. Vollhardt, *J. Am. Chem. Soc.* **1997**, *119*, 2052–2053; c) P. I. Dosa, C. Erben, V. S. Iyer, K. P. C. Vollhardt, I. M. Wasser, *J. Am. Chem. Soc.* **1999**, *121*, 10430–10431; d) M. Laskoski, W. Steffen, J. G. M. Morton, M. D. Smith, U. H. F. Bunz, *J. Am. Chem. Soc.* **2002**, *124*, 13814–13818.

[4] a) W. B. Wan, M. M. Haley, *J. Org. Chem.* **2001**, *66*, 3893–3901; b) J. A. Marsden, M. M. Haley, *J. Org. Chem.* **2005**, *70*, 10213–10226; c) T. Yoshimura, A. Inaba, M. Sonoda, K. Tahara, Y. Tobe, R. V. Williams, *Org. Lett.* **2006**, *8*, 2933–2936; d) K. Tahara, T. Yoshimura, M. Ohno, M. Sonoda, Y. Tobe, *Chem. Lett.* **2007**, *36*, 838–839.

[5] a) J. J. Pak, T. J. R. Weakley, M. M. Haley, *J. Am. Chem. Soc.* **1999**, *121*, 8182–8192; b) A. Sarkar, J. J. Pak, G. W. Rayfield, M. M. Haley, *J. Mater. Chem.* **2001**, *11*, 2943–2945; c) J. A. Marsden, J. J. Miller, M. M. Haley, *Angew. Chem.* **2004**, *116*, 1726–1729; *Angew. Chem. Int. Ed.* **2004**, *43*, 1694–1697; d) M. Sonoda, Y. Sakai, T. Yoshimura, Y. Tobe, K. Kamada, *Chem. Lett.* **2004**, *33*, 972–973; e) J. A. Marsden, J. J. Miller, L. D. Shirtcliff, M. M. Haley, *J. Am. Chem. Soc.* **2005**, *127*, 2464–2476; f) H. Enozawa, M. Hasegawa, D. Takamatsu, K. Fukui, M. Iyoda, *Org. Lett.* **2006**, *8*, 1917–1920; g) A. S. Andersson, K. Kilså, T. Hassenkam, J.-P. Gisselbrecht, C. Boudon, M. Gross, M. B. Nielsen, F. Diederich, *Chem. Eur. J.* **2006**, *12*, 8451–8459.

[6] T. Nishinaga, N. Nodera, Y. Miyata. K. Komatsu, *J. Org. Chem.* **2002**, *67*, 6091–6096.

[7] S. H. Seo, T. V. Jones, H. Seyler, J. O. Peters, T. H. Kim, J. Y. Chang, G. N. Tew, *J. Am. Chem. Soc.* **2006**, *128*, 9264–9265.

[8] S. H. Seo, J. Y. Chang, G. N. Tew, *Angew. Chem.* **2006**, *118*, 7688–7692; *Angew. Chem. Int. Ed.* **2006**, *45*, 7526–7530.

[9] K. Tahara, S. Furukawa, H. Uji-i, T. Uchino, T, Ichikawa, J. Zhang, W. Mamdouh, M. Sonoda, F. C. De Schryver, S. De Feyter, S. Y. Tobe, *J. Am. Chem. Soc.* **2006**, *128*, 16613–16625.

[10] For recent review, for example, see: a) C. D. Simpson, J. Wu, M. D. Watson, K. Müllen, *J. Mater. Chem.* **2004**, *14*, 494–504; b) J. M. Warman, M. P. de Haas, G. Dicker, F. C. Grozema, J. Piris, M. G. Debije, *Chem. Mater.* **2004**, *16*, 4600–4609; c) J. Wu, W. Pisula, K. Müllen, *Chem. Rev.* **2007**, *107*, 718–747; d) S. Sergeyev, W. Pisula, Y. H. Geerts, *Chem. Soc. Rev.* **2007**, *36*, 1902–1929.

[11] a) X. Dou, W. Pisula, J. Wu, G. J. Bodwell, K. Müllen, *Chem. Eur. J.* **2008**, *14*, 240–249.

[12] G. R. Desiraju, A. Gavezzotti, *Acta Crystallogr. Sect. A* **1989**, *45*, 473–482.

[13] I. Fischbach, T. Pakula, P. Minkin, A. Fechtenköltter, K. Müllen, H. W. Spiess, K. Saalwächter, *J. Phys. Chem. B* **2002**, *106*, 6408–6418.

[14] For example, see; a) A. K. Tripathi, M. Heinrich, T. Siegrist, J. Pflaum. *Adv. Mater.* **2007**, *19*, 2097–2101; b) H. Meng, F. Sun, M. B. Goldfinger, F. Gao, D. J. Londono, W. J. Marshal, G. S. Blackman, K. D. Dobbs, D. E. Keys. *J. Am. Chem. Soc.* **2006**, *128*, 9304–9305.

[15] For example, see: a) K. Kim, M. K. Kim, H. S. Kang, M. Y. Cho, J. Joo, J. H. Kim, K. H. Kim, C. S. Hong, D. H. Choi, *Synth. Met.* **2007**, *157*, 481–484; b) V. C. Sundar, J. Zaumseil, V. Podzorov, E. Menard, R. L. Willett, T. Someya, M. E. Gershenson, J. A. Rogers, *Science* **2004**, *303* 1644–1646.

[16] For example, see; a) A. L. Briseno, S. C. B. Mannsfeld, M. M. Ling, S. Liu, R. J. Tseng, C. Reese, M. E. Roberts, Y. Yang, F. Wudl, Z. Bao, *Nature* **2006**, *444*, 913–917; b) J. Y. Lee, S. Roth, Y. W. Park, *Appl. Phys. Lett.* **2006**, *88*, 252106/1–252106/3.

[17] For review. a) C. Reese, Z. Bao, *Mater. Today* **2007**, *10*, 20–27; b) R. W. I. de Boer, M. E. Gershenson, A. F. Morpurgo, V. Podzorov, *Phys. Status Solidi A* **2004**, *201*, 1302–1331.

[18] a) H. A. Staab, F. Graf, *Tetrahedron Lett.* **1966**, *7*, 751–757; b) I. D. Campbell, G. Eglinton, W. Henderson, R. A. Raphael, *J. Chem. Soc. D* **1966**, 87–89.

[19] H. Irngartinger, L. Leiserowitz, G. M. J. Schmidt, *Chem. Ber.* 1970, ***103***, 1119–1131.

[20] G. R. Desiraju, *Angew. Chem.* **1995**, *107*, 2541–2558; *Angew. Chem. Int. Ed. Engl.* 1995, ***34***, 2311–2327.

[21] a) Y. Mizobe, T. Tohnai, M. Miyata, Y. Hasegawa, *Chem. Commun.* **2005**, 1839–1841; b) Y. Mizobe, H. Ito, I. Hisaki, M. Miyata, Y. Hasegawa, N. Tohnai, *Chem. Commun.* **2006**, 2126–2128.

[22] A. J. Matzger, M. Shim, K. P. C. Vollhardt, *Chem. Commun.* **1999**, 1871–1872.

[23] D. B. Kimball, T. J. R. Weakley, M. M. Haley, *J. Org. Chem.* **2002**, *67*, 6395–6405.

[24] M. Iyoda, S. Sirinintasak, Y. Nishiyama, A. Vorasingha, F. Sultana, K. Nakao, Y. Kuwatani, H. Matsuyama, M. Yoshida, Y. Miyake, *Synthesis* **2004**, *9*, 1527–1531.

[25] Although the crystal structure is essentially same with that reported by Schmidt (see ref. [19], Refcode: TBZDTY01), cell parameters in the crystal data were renewed, see Experimental Section.

[26] a) M. A. Spackman, P. G. Byrom, *Chem. Phys. Lett.* **1997**, *267*, 215–220; b) J. J. McKinnon, A. S. Mitchell, M. A. Spackman, *Chem. Eur. J.* **1998**, *4*, 2136–2141; c) J. J. McKinnon, M. A. Spackman, A. S. Mitchell, *Acta Crystallogr. Sect. B* **2004**, *60*, 627–668.

[27] Gaussian 03 (Revision D.01), M. J. Frisch, G. W. Trucks, H. B. Schlegel, G. E. Scuseria, M. A. Robb, J. R. Cheeseman, J. A. Montgomery Jr., T. Vreven, K. N. Kudin, J. C. Burant, J. M. Millam, S. S. Iyengar, J. Tomasi, V. Barone, B. Mennucci, M. Cossi, G. Scalmani, N. Rega, G. A. Petersson, H. Nakatsuji, M. Hada, M. Ehara, K. Toyota, R. Fukuda, J. Hasegawa, M. Ishida, T. Nakajima, Y. Honda, O. Kitao, H. Nakai, M. Klene, X. Li, J. E. Knox, H. P. Hratchian, J. B. Cross, C. Adamo, J. Jaramillo, R. Gomperts, R. E. Stratmann, O. Yazyev, A. J. Austin, R. Cammi, C. Pomelli, J. W. Ochterski, P. Y. Ayala, K. Morokuma, G. A. Voth, P. Salvador, J. J. Dannenberg, V. G. Zakrzewski, S. Dapprich, A. D. Daniels, M. C. Strain, O. Farkas, D. K. Malick, A. D. Rabuck, K. Raghavachari, J. B. Foresman, J. V. Ortiz, Q. Cui, A. G. Baboul, S. Clifford, J. Cioslowski, B. B. Stefanov, G. Liu, A. Liashenko, P. Piskorz, I. Komaromi, R. L. Martin, D. J. Fox, T. Keith, M. A. Al-Laham, C. Y. Peng, A. Nanayakkara, M. Challacombe, P. M. W. Gill, B. Johnson, W. Chen, M. W. Wong, C. Gonzalez, J. A. Pople, Gaussian, Inc., Pittsburgh, PA, **2004**.

[28] a) M. Guillaume, B. Champagne, F. Zutterman, *J. Phys. Chem. A* **2006**, *110*, 13007–13013; b) B. Champagne, M. Guillaume, F. Zutterman, *Chem. Phys. Lett.* **2006**, *425*, 105–109 and references therein.

[29] In the present system, the DMSO molecules in crystal **2**•3DMSO do not affect on the TRMC measurement because molecular rotation is restricted, and thus, inactive toward irradiated microwave.

[30] a) S. Seki, Y. Yoshida, S. Tagawa, K. Asai, K. Ishigure, K. Furukawa, M. Fujiki, N. Matsumoto, *Philos. Mag. B* **1999**, *79*, 1631–1645; b) F. C. Grozema, L. D. A. Siebbeles, J. M. Warman, S. Seki, S. Tagawa, U. Scherf, *Adv. Mater.* **2002**, *14*, 228–231; c) A. Saeki, S. Seki, T. Sunagawa, K. Usida, S. Tagawa, *Philos. Mag. B* **2006**, *86*, 1261–1276; d) Y. Yamamoto, T. Fukushima, W. Jin, A. Kosaka, T. Hara, T. Nakamura, A. Saeki, S. Seki, S. Tagawa, T. Aida, *Adv. Mater.* **2006**, *18*, 1297–1300; e) A. Saeki, S. Seki, T. Takenobu, Y. Iwasa, S. Tagawa, *Adv. Mater.* **2008**, *20*, 920–923.

[31] a) A. M. van de Craats, J. M. Warman, K. Müllen, Y. Geerts, J. D. Brand, *Adv. Mater.* **1998**, *10*, 36–38; b) A. M. van de Craats, J. M. Warman, A. Fechtenkötter, J. D. Brand, M. A. Harbison, K. Müllen, *Adv. Mater.* **1999**, *11*, 1469–1472; c) W. Pisula, A. Menon, M. Stepputat, I. Lieberwith, U. Kolb, A. Tracz, H. Sirringhaus, T. Pakula, K. Müllen, *Adv. Mater.* **2005**, *17*, 684–689.

[32] The value of ϕ determined by DC-CI experiment under high electric field strength ($1.6\times10^4\,V\,cm^{-1}$) is probably overestimated. There-

fore, the actual value of the mobilities may be larger than that determined in this study.

[33] Although the FP-TRMC measurement of the single crystal of rubrene gave the mobility of $5.2\times10^{-2}\,cm^2V^{-1}s^{-1}$ as shown in the literature of reference [31e], the value is approximately three orders of magnitude smaller than reported highest FET mobility for the rebrene single crystal. In connection with this discrepancy, several reasons including underestimation of the extinction coefficients of charged species in the crystal phase have been speculated. Thus, the value is expected to be minimum value of the mobility of rubrene single crystal.

[34] A. Altomare, M. Burla, M. Camalli, G. Cascarano, C. Giacovazzo, A. Guagliardi, A. Moliterni, G. Polidori, R. Spagna, *J. Appl. Crystallogr.* **1999**, *32*, 115–119.

[35] CrystalStructure 3.8, Crystal Structure Analysis Package, Rigaku and Rigaku Americas (2000–2007): The Woodlands.

[36] G. M. Sheldrick, SHELXL-97, Program for crystal structure refinement, University of Göttingen (Germany), **1997**.

Received: February 5, 2008
Published online: April 9, 2008

